International Journal of
Automotive Manufacturing and Materials（IJAMM）

Scilight

Review

Active Disturbance Rejection Control Using a Phase Optimized Extended State Observer for a Nanopositioner

Wei Wei [1,*], Pengfei Xia [2], and Min Zuo [3]

[1] School of Intelligent Engineering and Automation, Beijing University of Posts and Telecommunications, Beijing 100876, China
[2] School of Automation, Beihang University, Beijing 100191, China
[3] School of Computer and Information Engineering, Beijing Technology and Business University, Beijing 100048, China
* Correspondence: weiweizdh@126.com
Received: 5 April 2024; Revised: 9 June 2024; Accepted: 12 June 2024; Published: 28 June 2024

Abstract: A piezoelectric actuator is commonly utilized in nanopositioning for its stiffness, fast response, and ultrahigh precision. However, hysteresis in piezoelectric materials dramatically degrades system performance. By introducing a straightforward and effective modification to a classical extended state observer, a phase-optimized extended state observer is proposed to provide a phase-leading estimation of the generalized disturbance. Accordingly, a phase-optimized active disturbance rejection control is designed, and much more satisfied performance can be guaranteed. Convergence of the phase-optimized extended state observer and closed-loop stability of the phase-optimized active disturbance rejection control have been analyzed. Moreover, steady-state estimation error and phase-leading property have been proved. Advantages of the phase optimized active disturbance rejection control over the PI and the active disturbance rejection control are confirmed. Experimental results show that the phase-optimized active disturbance rejection control can achieve more desired disturbance rejection and motion tracking.

Keywords: active disturbance rejection control; hysteresis; phase optimized extended state observer; piezoelectric actuators; positioning

1. Introduction

Motion systems driven by piezoelectric actuators (PEAs) have numerous advantages, like nanometer resolution, rapid response, and large output force [1]. They have been widely utilized in different fields, such as micromanipulators, atomic force microscopes, and ultra-precision machines [2]. However, hysteresis in PEAs dramatically degrades positioning accuracy [3]. To address it, hysteresis models are constructed. For example, a Prandtl-Ishlinskii model (PIM) [4] and a modified PIM [5] for asymmetric hysteresis have been presented. A Hammerstein-like structure has also been utilized to describe a piezoelectric-actuated stage, and a new modeling approach is proposed [6]. Based on those models, numerous model-based techniques have been designed to promote precision and speed of the stages. One common way is to build an inverse hysteresis model to compensate the hysteresis. By taking an adaptive strategy to eliminate the accumulated error, an improved inverse model has been presented [7]. An inverse Bouc-Wen model connected an iterative learning controller was also designed to compensate both nonlinearities and uncertainties [8]. Another approach is to directly employ hysteresis models to serve as feedforward compensators. Bouc-Wen modeling and inverse multiplicative structure have been taken to compensate the hysteresis [9]. A generalized Duhem model has also been used to realize the feedforward compensation [10].

It is known that the model-based methods take effect when system models are consistent with system dynamics. However, hysteresis, a typical amplitude and frequency-dependent phenomenon [2], depends

heavily on both amplitude and frequency of an input signal. It is difficult to build a faithful model. Naturally, positioning accuracy degrades remarkably if those model-based approaches are still utilized. To effectively address the hysteresis, control techniques, which are less dependent on system model and robust enough to external disturbances, can guarantee the closed-loop performance and they are in great need. Numerous efforts [11–13] (and references therein) have been made. For the positioning stage, a finite-time learning control [14] was proposed to reduce the requirements on system model to improve the positioning, a decomposition-learning-based output tracking approach [15] was designed to address the robustness of the output tracking, and a neural networks-based learning algorithm [16] was developed to deal with uncertainties in a piezoelectric positioning system in an online way.

Active disturbance rejection control (ADRC) [17], proposed by Han in 1990s, is a unique way to address uncertainties and disturbances. From the viewpoint of the ADRC, all undesired factors, such as perturbations of system parameters, un-modeled dynamics, and external uncertain disturbances, are regarded as generalized disturbance. Furthermore, the generalized disturbance is defined as a new state, i. e., the extended state. Then, an extended state observer (ESO) is designed to reconstruct system states and the extended state. Taking advantage of the reconstructed extended state, the ADRC can compensate disturbance before it corrupts system outputs. In other words, control action of the ADRC is more active, and the closed-loop system is robust enough. For advantages of the ADRC, it has been exploited in many occasions, such as thermodynamic systems [18], hypersonic vehicles [19], powered parafoils [20], oxygen masks [21], high-purity distillation columns [22], and nano-positioning systems [23–25].

Although the ADRC effectively deals with uncertainties and disturbances, it still needs to be enhanced. For example, theoretically, a classical ESO can estimate a constant disturbance without steady-state error [26]. However, in reconstructing a time-varying disturbance, the steady-state estimation errors still exist, even if they may be acceptable in engineering. That is the insufficiency of a classical ESO, since the disturbance is seldom constant. The powerlessness in reconstructing a time-varying disturbance limits the ADRC. To address it, increasing the order of an ESO [26–28] and introducing nonlinearities [29] are commonly utilized. Satisfied estimations can be obtained, but the shortcomings are also apparent. First, it is under the assumption that the generalized disturbance is m-th order differentiable [26]. Second, it is the computational complexity of a modified ESO [26]. Therefore, it is necessary to design an optimized ESO to get a more desirable reconstruction.

In this article, a classical ESO, which makes the ADRC reject disturbance actively, is optimized to estimate the generalized disturbance timelier and more actively. Unlike our previous work [30], a phase optimization law (POL) is proposed and seamlessly incorporated into a classical ESO. Then, without introducing any linearity or nonlinearity, a phase-optimized ESO (POESO) can be obtained more conveniently and a timelier and more active generalized disturbance estimation is achieved. Accordingly, control action of the ADRC becomes more active and the closed-loop performance is promoted notably. The main contributions are listed below:

(1) The estimation phase greatly decides the closed-loop performance of the ADRC. To reduce the phase delay of the generalized disturbance estimation, a phase optimization law is proposed.

(2) A POESO is proposed, and based on the POESO, a phase-optimized active disturbance rejection control (POADRC) is presented.

(3) Theoretically, the advantages of the POESO on both phases and steady-state estimation errors are confirmed. Moreover, to achieve an optimized generalized disturbance estimation phase, a solid guidance on determining the adjustable POL parameter is obtained via the final-value theorem.

(4) Based on a positioner, comparisons and evaluations under different scenarios are performed. The advantages of the POESO and the POADRC have been testified via experimental results.

The remainder of this article is organized as follows. In Section 2, a positioning stage is described and the problem is presented. The POESO is proposed, and the POADRC is designed in Section 3. The convergence of the POESO, closed-loop stability of the POADRC, steady-state estimation errors of the POESO, and the advantage of the POESO are also discussed. Section 4 presents experimental results. Finally, Section 5 presents the conclusion.

2. Experimental Setup and Problem Statements

2.1. Experimental Setup

A positioning stage shown in Figure 1 is employed. PEAs drive the stage, and it is connected to a voltage amplifier. Horizontal movements of the stage are up to 100 μm. The resonant frequency of the stage is 190 Hz. Output displacements are measured by a built-in capacitive displacement sensor, whose resolution is 0.8 nm. A host computer controls a hardware-in-the-loop system, which produces voltages to drive the stage.

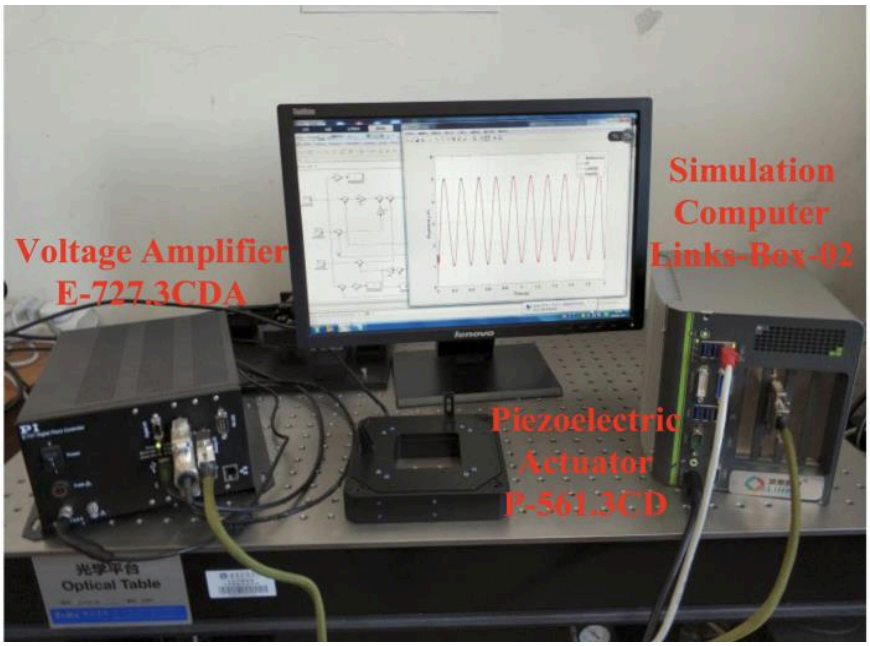

Figure 1. Experiment setup.

2.2. Problem Statements

Hysteresis is a typical nonlinearity in a PEA. It is an amplitude and rate-dependent nonlinear behavior [1,2]. Applying inputs with different amplitudes and frequencies, one has Figure 2. It presents amplitude and rate dependencies of the hysteresis. Figure 2a shows that the displacements of the system depend upon not only current inputs but also historical input voltages. In Figure 2b, it can be observed that the hysteresis becomes more conspicuous with an increasing input frequency. Thus, the hysteresis is complex and cannot be accurately described by a mathematical model. Therefore, if the hysteresis is not addressed effectively and efficiently, it definitely seriously degrades positioning speed, and accuracy, or even destabilizes a closed-loop system [1,2,15,16]. In other words, the hysteresis challenges the precise control of a stage driven by PEAs. To minimize the influence of the hysteresis, an effective and efficient technique, which is less dependent on the hysteresis model and can suppress the hysteresis, is in great need.

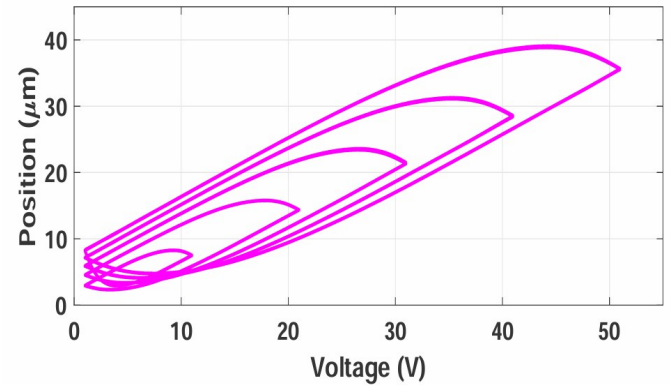

(**a**)

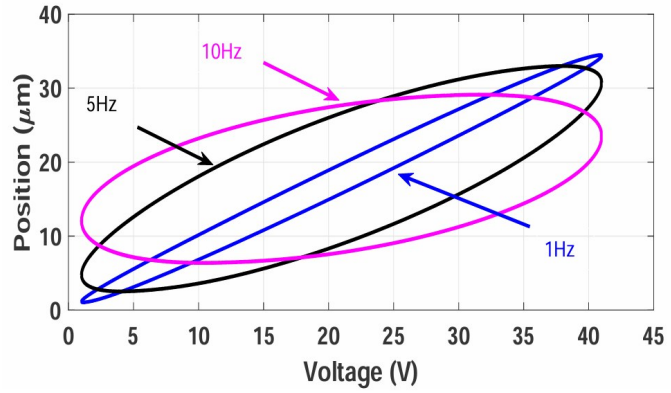

(**b**)

Figure 2. Hysteresis. (**a**) amplitude-dependent behaviors and (**b**) rate-dependent behaviors.

3. Phase Optimized Active Disturbance Rejection Control

Rather than model the hysteresis, viewing it as a part of the generalized disturbance, one can reconstruct and cancel it out. Moreover, a timelier and more active generalized disturbance estimation is crucial in achieving more satisfied closed-loop tracking performance. Thus, given that a leading estimation phase promises a more active estimation, a phase optimization law (POL) is proposed here. Based on the POL, a POESO is designed to provide a timelier and more active generalized disturbance estimation. Then, a POADRC can be constructed, and a timelier and more active control signal is obtained. In addition, due to the less dependent on the stage model and more active estimation and control, the proposed POESO and the POADRC are more effective and practical in controlling a positioning stage driven by PEAs.

3.1. The POESO

For a second-order system

$$\ddot{y} = F\left(y, \dot{y}, w\right) + bu \tag{1}$$

where u is a control signal, y is the system output, w includes hysteresis, model uncertainties and external disturbances, $F\left(y, \dot{y}, w\right)$ is a nonlinear function representing system dynamics, and b is an unknown control gain.

Let $x_1 = y, x_2 = \dot{y}$, and $f\left(y, \dot{y}, w\right) = F\left(y, \dot{y}, w\right) + \left(b - b_0\right)u$. In ADRC, $f\left(y, \dot{y}, w\right)$ is defined to be a generalized disturbance. It includes all dynamics that differ from a pure integrator chain. Let f be an extended state, i.e., $x_3 = f\left(y, \dot{y}, w\right)$. Then, system (1) can be rewritten as

$$\begin{cases} \dot{x}_1 = x_2 \\ \dot{x}_2 = x_3 + b_0 u \\ \dot{x}_3 = h \\ y = x_1 \end{cases} \tag{2}$$

where x_1, x_2 and x_3 are system states, h is the derivative of f, and b_0 is an adjustable parameter.

For system (2), a classical ESO can be designed as

$$\begin{cases} \dot{z}_1 = z_2 - \beta_1 (z_1 - y) \\ \dot{z}_2 = z_3 - \beta_2 (z_1 - y) + b_0 u \\ \dot{z}_3 = -\beta_3 (z_1 - y) \end{cases} \tag{3}$$

where z_1, z_2 and z_3 are outputs of an ESO, β_1, β_2 and β_3 are adjustable observer gains. The ESO works, i.e., $z_1 \to y, z_2 \to \dot{y}$, and $z_3 \to f(y, \dot{y}, w)$, if proper gains are selected.

However, the ESO (3) can only estimate a constant disturbance without steady-state error. It is not efficient enough. To address this, instead of increasing the order or introducing nonlinear functions to a classical ESO, a linear POL is proposed.

$$z_{3PO} = z_3 + \frac{1}{c} \dot{z}_3 \tag{4}$$

where z_{PO} is an optimized generalized disturbance estimation, c is an adjustable gain. If c tends to infinity, a POESO degrades into a classical ESO. Therefore, c plays a key role in phase optimization.

Remark 1. *In the POL (4), a differential operation is introduced. However, it does not result in a noise amplification, since, from the ESO (3), one can get* $\dot{z}_3$ *by* $-\beta_3 (z_1 - y)$ *without differentiating any signal.*

By introducing the POL, a POESO can be designed as

$$\begin{cases} \dot{z}_1 = z_2 - \beta_1 (z_1 - y) \\ \dot{z}_2 = z_3 - \beta_2 (z_1 - y) + b_0 u \\ \dot{z}_3 = -\beta_3 (z_1 - y) \\ z_{3PO} = z_3 + (\dot{z}_3 / c) \end{cases} \tag{5}$$

Remark 2. *The optimization in a POESO means a timelier and more active generalized disturbance estimation can be obtained* by *taking a proper c. Although it is not a typical optimization problem, and an adequate parameter to get an optimized generalized disturbance estimation phase can be fixed by guidance or through trial and error, it is still an optimized process. In following sections, it can be seen clearly that such a phase-leading design does improve an ESO on estimating the time-varying disturbance if a proper c is chosen.*

3.2. The POADRC

Based on the POESO, a control law of the POADRC is

$$u = \frac{k_p (r - z_1) + k_d (\dot{r} - z_2) + (\ddot{r} - z_{3PO})}{b_0} \tag{6}$$

where $r, \dot{r}$ are set-value and its derivative, k_p, k_d are controller gains, z_1, z_2 and z_{3PO} are outputs of a POESO, b_0 is an adjustable parameter. Figure 3 presents a block diagram of the POADRC.

Figure 3 shows that the POADRC comprises a control law and a POESO. The POESO includes an ESO and a POL. It is worth pointing out that a POESO is constructed by a direct modification based on a classical ESO rather than introducing linearities, nonlinearities or increase its order. Therefore, a POESO can be obtained directly based on a classical ESO. In other words, it is a practical technique to improve the

generalized disturbance estimation, although its convergence and advantages presented in the following sections seem a little obscure.

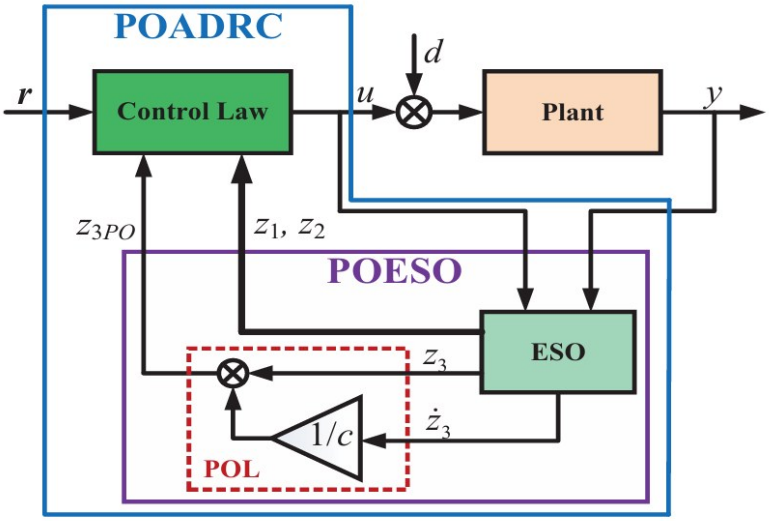

Figure 3. Block diagram of the POADRC.

Similar to Ref. [31], adjustable controller gains and observer gains can be selected. The adjustable gain c is chosen based on the final-value theorem (see Section 3.5). Then

$$k_p = \omega_c^2, k_d = 2\omega_c \tag{7}$$

$$\beta_1 = 3\omega_o, \beta_2 = 3\omega_o^2, \beta_3 = \omega_o^3, c = \beta_3/\beta_2 = \omega_o/3 \tag{8}$$

where ω_c, ω_o are controller bandwidth and observer bandwidth, respectively.

Remark 3. *With the help of a POESO, the POADRC produces a more effective and efficient control signal to drive the positioning stage to track the reference timelier and more accurately. It is not necessary to get an accurate model of the complex hysteresis. However, if some model information is also available, it will definitely help improve the positioning performance. Thus, it is practical to address the hysteresis.*

3.3. Convergence of the POESO

Let estimation errors $e_i(t) = z_i(t) - x_i(t), i = 1, 2,$ and $e_{3PO}(t) = z_{3PO}(t) - x_3(t)$. From (2) and (5), the estimation error dynamics of the POESO is

$$\begin{cases} \dot{e}_1(t) = e_2(t) - \beta_1 e_1(t) \\ \dot{e}_2(t) = e_{3PO}(t) + \left(\dfrac{\beta_3}{c} - \beta_2\right) e_1(t) \\ \dot{e}_{3PO}(t) = -h(t) - \dfrac{\beta_3}{c} e_2(t) + \left(\dfrac{\beta_1\beta_3}{c} - \beta_3\right) e_1(t) \end{cases} \tag{9}$$

For convenience, let $\varepsilon_i(t) = e_i(t)/\omega_o^{i-1}, i = 1, 2, \varepsilon_{3PO}(t) = e_{3PO}(t)/\omega_o^2, \varepsilon_{PO}(t) = \left[\varepsilon_1(t), \varepsilon_2(t), \varepsilon_{3PO}(t)\right]^T$ and $\dot{\varepsilon}_{PO}(t) = \left[\dot{\varepsilon}_1(t), \dot{\varepsilon}_2(t), \dot{\varepsilon}_{3PO}(t)\right]^T$. Considering (7) and (8), one can rewrite (9) as

$$\dot{\varepsilon}_{PO}(t) = \omega_o \mathbf{A}_\varepsilon \varepsilon_{PO}(t) + \mathbf{B}_\varepsilon \frac{h(t)}{\omega_o^2} \tag{10}$$

where

$$\mathbf{A}_\varepsilon = \begin{bmatrix} -3 & 1 & 0 \\ 0 & 0 & 1 \\ 8 & -3 & 0 \end{bmatrix}, \mathbf{B}_\varepsilon = \begin{bmatrix} 0 \\ 0 \\ -1 \end{bmatrix}$$

Theorem 1. *Assuming that $h(t)$ is bounded, there exist constants $\sigma_i > 0$ and a finite time $T_1 > 0$ such that $|e_i(t)| \le \sigma_i, i = 1, 2, |e_{3PO}(t)| \le \sigma_3, \forall t \ge T_1 > 0$ and $\omega_o > 0$. Furthermore, $\sigma_i = O(1/\omega_o^k)$ for some positive integer k.*

Theorem 1 shows that the estimation errors of the POESO are bounded and the upper bounds decrease with increasing ω_o.

Remark 4. *According to* [32] *the change rate in a physical world is limited or no change is instantaneous. For a positioning stage, it is also reasonable since no positioning stage will change abruptly. Thus, here, $h(t)$ is assumed to be bounded.*

Remark 5. *In fact, a relatively mild assumption and a more rigorous stability proof is available in* [33]. *However, the assumption on $h(t)$ is intuitive, and it does not violate physical laws. Moreover, it can be easily accepted by engineers.*

3.4. Closed-Loop Stability of the POADRC

Let $r = [r_1, r_2, r_3]^T = [r, \dot{r}, \ddot{r}]^T$ and tracking errors $\xi_i(t) = r_i(t) - x_i(t), i = 1, 2$. Theorem 2 can be obtained.

Theorem 2. *There exist constants $\mu_i > 0$ and a finite time $T_3 > 0$ such that $|\xi_i(t)| \le \mu_i, i = 1, 2, \forall t \ge T_3 > 0, \omega_o > 0$ and $\omega_c > 0$. Furthermore, $\mu_i = O(1/\omega_c^q)$ for some positive integer q.*

Thus, its output is also bounded for a bounded reference. That is, the closed-loop system is bounded input and bounded output (BIBO) stable. Enlarging the controller bandwidth ω_c can reduce the tracking errors ξ_i. In addition, the Appendix shows that minimizing $\sigma_i (i = 1, 2, 3)$ also helps reduce ξ_i.

Remark 6. *One cannot get the unknown control gain b, but an adjustable control gain b_0 can be set in advance. The difference between b and b_0 is viewed as a part of the generalized disturbance. The estimation error is convergent as long as the observer bandwidth is enough (Theorem 1). Based on the convergence of the POESO, tracking errors converge under a proper controller bandwidth (Theorem 2). Therefore, the unknown control gain b can be addressed effectively by a POESO, and the closed-loop stability can also be guaranteed.*

3.5. Comparisons of the Steady-State Estimation Errors

Taking Laplace transformation on both sides of (3) and (5) and considering (8), one has

$$z_1 = \frac{3\omega_o s^2 + 3\omega_o^2 s + {\omega_o}^3}{(s+\omega_o)^3} y + \frac{b_0 s}{(s+\omega_o)^3} u \tag{11}$$

$$z_2 = \frac{3\omega_o^2 s^2 + {\omega_o}^3 s}{(s+\omega_o)^3} y + \frac{b_0 (s^2 + 3\omega_o s)}{(s+\omega_o)^3} u \tag{12}$$

$$z_3 = \frac{{\omega_o}^3 s^2}{(s+\omega_o)^3} y - \frac{b_0 \omega_o^3}{(s+\omega_o)^3} u \tag{13}$$

$$z_{3PO} = \frac{\omega_o^3 s^3/c + \omega_o^3 s^2}{(s+\omega_o)^3} y - \frac{b_0 \omega_o^3 s/c + b_0 \omega_o^3}{(s+\omega_o)^3} u \tag{14}$$

then estimation errors e_1, e_2, e_3 and e_{3PO} are

$$e_1 = -\frac{s^3}{\left(s+\omega_o\right)^3} y + \frac{b_0 s}{\left(s+\omega_o\right)^3} u \tag{15}$$

$$e_2 = -\frac{s^4+3\omega_o s^3}{\left(s+\omega_o\right)^3} y + \frac{b_0\left(s^2+3\omega_o s\right)}{\left(s+\omega_o\right)^3} u \tag{16}$$

$$e_3 = b_0\left[1-\frac{\omega_o^3}{\left(s+\omega_o\right)^3}\right]u - \left[1-\frac{\omega_o^3}{\left(s+\omega_o\right)^3}\right]s^2 y \tag{17}$$

$$e_{3PO} = b_0\left[1-\frac{\omega_o^3 s/c+\omega_o^3}{\left(s+\omega_o\right)^3}\right]u - \left[1-\frac{\omega_o^3 s/c+\omega_o^3}{\left(s+\omega_o\right)^3}\right]s^2 y \tag{18}$$

In addition, system (2) can be rewritten as

$$\ddot{y} = f + b_0 u \tag{19}$$

then

$$e_3 = \left[\frac{\omega_o^3}{\left(s+\omega_o\right)^3} - 1\right] f \tag{20}$$

$$e_{3PO} = \left[\frac{\omega_o^3 s/c+\omega_o^3}{\left(s+\omega_o\right)^3} - 1\right] f \tag{21}$$

When f is a step signal whose amplitude is K, i.e., $f(s) = K/s$, then steady-state estimation errors of z_3 and z_{3PO} are

$$\begin{cases} e_{3s} = \lim\limits_{s\to 0} \; se_3 = 0 \\ e_{3POs} = \lim\limits_{s\to 0} \; se_{3PO} = 0 \end{cases} \tag{22}$$

It shows that, for a constant disturbance, both an ESO and a POESO have no steady-state estimation errors no matter what c is.

For (21), let $c = \omega_o/3$, and it follows

$$e_{3PO} = -\frac{s^3+3\omega_o s^2}{\left(s+\omega_o\right)^3} f \tag{23}$$

When f is a ramp signal with amplitude K_1, i.e., $f(s) = K_1/s^2$, steady-state estimation errors of z_3 and z_{3PO} are

$$\begin{cases} e_{3s} = \lim\limits_{s\to 0} \; se_3 = -\dfrac{3K_1}{\omega_o} \\ e_{3POs} = \lim\limits_{s\to 0} \; se_{3PO} = 0 \end{cases} \tag{24}$$

It means that a POESO still has zero steady-state estimation error in presence of a ramp disturbance. By contrast, the steady-state estimation error still exists in a classical ESO.

When f is a sinusoidal signal, amplitude frequency characteristics of (20) and (23) are

$$\begin{cases} \left|e_3(j\omega)\right| = \left|\dfrac{\left(3\omega_o^2\omega^4 + 9\omega_o^4\omega^2 + \omega^6\right)^{1/2}}{\left(\omega_o^2 + \omega^2\right)^{3/2}}\right| \left|f(j\omega)\right| \\ \left|e_{3PO}(j\omega)\right| = \left|\dfrac{\left(9\omega_o^2\omega^4 + \omega^6\right)^{1/2}}{\left(\omega_o^2 + \omega^2\right)^{3/2}}\right| \left|f(j\omega)\right| \end{cases} \tag{25}$$

As long as the numerator of $\left|e_3(j\omega)\right|$ is larger than the one of $\left|e_{3PO}(j\omega)\right|$, i. e., $3\omega_o^2 > 2\omega^2$, one has $\left|e_3(j\omega)\right| > \left|e_{3PO}(j\omega)\right|$ in a large frequency range. It indicates that a POESO rejects the sinusoidal disturbance much better.

From the analyses, one can see that a POESO is definitely superior to an ESO on reconstructing a time-varying disturbance.

3.6. Essence of a POESO outperforming an ESO

In this part, the advantage of a POESO is analyzed. Replacing *s* with *jw* in (20) and (23), one has phase frequency characteristics of the generalized disturbance estimation errors

$$\begin{cases} \psi_{e_3} = \arctan\dfrac{\omega^2 - 3\omega_o^2}{3\omega_o\omega} - \angle\left(\omega_o + j\omega\right)^3 + \angle f(j\omega) \\ \psi_{e_{3PO}} = \arctan\dfrac{\omega}{3\omega_o} - \angle\left(\omega_o + j\omega\right)^3 + \angle f(j\omega) \end{cases} \tag{26}$$

where ψ_{e_3} is the phase frequency characteristic of an ESO's the generalized disturbance estimation error, and $\psi_{e_{3PO}}$ is the phase frequency characteristic of a POESO's the generalized disturbance estimation error.

Considering that the phase difference between the generalized disturbance estimation errors is just the phase difference between the generalized disturbance estimations, one can determine the latter by calculating $\Delta\psi$, here

$$\Delta\psi = \psi_{e_{3PO}} - \psi_{e_3} = \arctan\frac{9\omega_o^3}{6\omega_o^2\omega + \omega^3} \tag{27}$$

Since $\left(9\omega_o^3\right)\cdot\left(6\omega_o^2\omega + \omega^3\right)^{-1} >, \Delta\psi = \psi_{e_{3PO}} - \psi_{e_3} > 0$. Thus, the phase of z_{3PO} always leads the one of z_3. This is the essence that a POESO is more active and effective.

4. Hardware Tests

In this section, hardware tests are performed to confirm the proposed POESO and POADRC. Three references are considered. A step reference is taken to verify the constant reference tracking. Another two references are both sinusoidal signals. One is selected to check the time-varying reference tracking, the other is utilized to examine the high-bandwidth tracking. Experiments are performed on the platform shown in Figure 1. The POADRC is designed as given in Figure 3. Parameters of the PI, the ADRC, and the POADRC are given in Table 1. References, disturbances and their descriptions are listed in Table 2. ADRC and POADRC take same ω_c, ω_o, and b_0 to get impartial comparisons. The sampling interval is set to be 0.05 ms.

Additionally, in light of the generalized disturbance is not available in hardware experiments, advantage of the POESO is visualized by its leading generalized disturbance estimation.

Table 1. Parameters of the ADRC and the POADRC.

	PI		**ADRC**			**POADRC**			
References	***P***	***I***	ω_c **(rad/s)**	ω_o **(rad/s)**	b_0	ω_c **(rad/s)**	ω_o **(rad/s)**	b_0	***c***
r_1	0.01	1.3	80	100	3×10^4	80	100	3×10^4	18
r_2	2	50	2000	1155	1×10^6	2000	1155	1×10^6	385
r_3	2	60	4000	1500	1×10^6	4000	1500	1×10^6	500

Table 2. Signals and Descriptions.

Signals	Descriptions (Unit: μm)	
References	$r_1 = 4$	
	$r_2 = 2sin(10\pi t - 0.5\pi) + 3$	
	$r_3 = 0.5sin(40\pi t - 0.5\pi) + 3.5$	
Disturbances	0.1	$0.5 \leqslant t < 1$
	$0.2(t - 1) + 0.1$	$1 \leqslant t < 1.5$
	$0.1sin(8\pi t + 0.5\pi) + 0.1$	$1.5 \leqslant t < 2$

4.1. Step Responses

Set-point tracking and the disturbance rejection ability have been examined. To make fair comparisons, PI and ADRC are tuned to achieve similar rising time. Results are shown in Figure 4. Responses of the PI and ADRC rise to 2% of the set-value at around 0.24 s, and the POADRC needs about 0.1167 s. In presence of a constant-type disturbance, dynamic falls of the PI, ADRC and POADRC are 0.7267, 0.3410, and 0.2008 μm, respectively. Their recovery time are 0.2514, 0.2380, and 0.1294 s, separately. For a ramp disturbance, the maximum positioning error (MPE) of the PI, ADRC and POADRC are 0.1797, 0.1026, and 0.0535 μm. For a sine disturbance, their MPEs are 0.9931, 0.4532, and 0.2639 μm. Control efforts are shown in Figure 4c. Root mean square (RMS) values of control signals generated by the PI, ADRC, and POADRC are 0.3763, 0.3735, and 0.3753. Obviously, the ADRC consumes least energy. By contrast, POADRC responds faster, and it requires just a little more energy. However, from 0.5 to 2 s, in presence of external disturbances, RMS values of the control signals are 0.3862, 0.3804, and 0.3782. It means that the POADRC consumes least energy in rejecting disturbances.

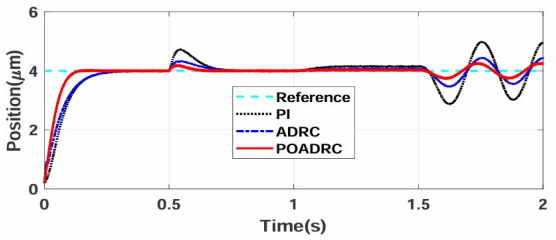

(**a**)

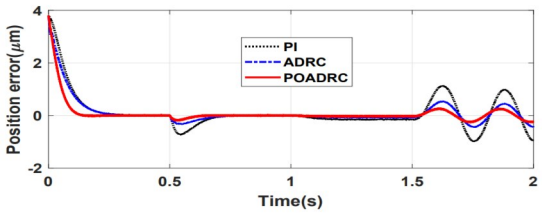

(**b**)

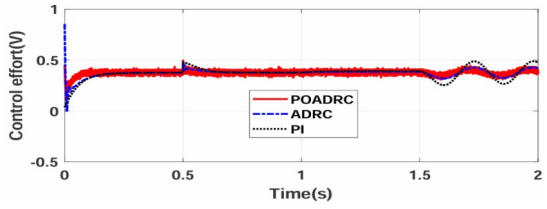

(**c**)

Figure 4. Step responses. (**a**) Position tracking results. (**b**) Position tracking errors. (**c**) Control efforts.

Usually, dynamic falls, MPEs and recover times are utilized to evaluate step responses in presence of external disturbances. Here, they are also employed and their values are summarized in Figure 5. They are consistent with Figure 4 and more concrete. RMS values are listed in Table 3. Δ_1%is percentage of the RMS value produced by the POADRC over the one produced by the PI, and Δ_2% represents percentage of the RMS value generated by the POADRC over the one generated by the ADRC. A negative percentage means the value of the POADRC is increased. Otherwise, it indicates that the corresponding value of the POADRC is decreased. Figure 6 shows that the generalized disturbance estimation phase of a POESO always leads the one of a classical ESO. Considering the data in the figures, we conclude that the POADRC has better tracking response and disturbance rejection, since much faster and more accurate disturbance estimation are guaranteed by a POESO.

Table 3. RMS values of the Three Controllers.

References	Indexes	PI	ADRC	POADRC	Δ_1%	Δ_2%
Step	RMS error (μm)	0.6914	0.5241	0.4199	39.30%	19.90%
	RMS control (V)	0.3763	0.3735	0.3753	0.27%	−0.48%
5 Hz Sine	RMS error (μm)	0.0770	0.0467	0.0417	45.80%	10.70%
	RMS control (V)	0.3284	0.3278	0.3268	0.49%	0.31%
20 Hz Sine	RMS error (μm)	0.0670	0.0372	0.0179	73.30%	51.90%
	RMS control(V)	0.3521	0.3560	0.3530	−0.26%	0.84%

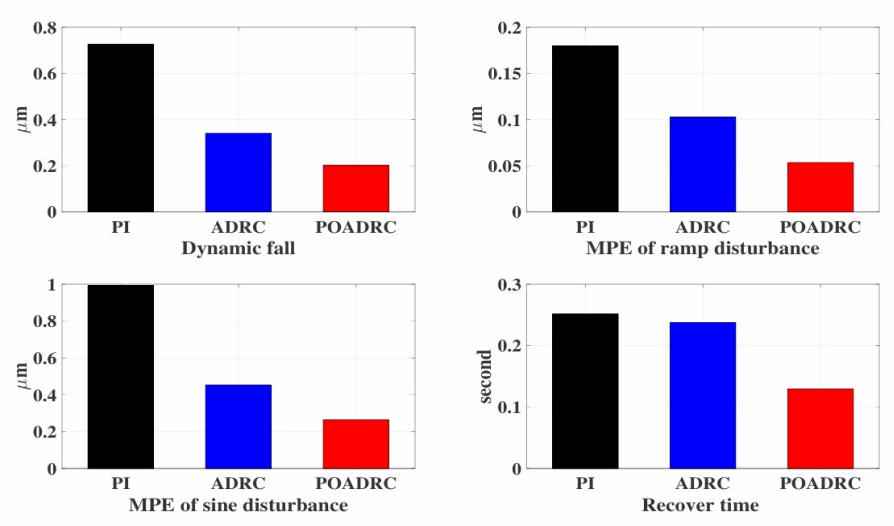

Figure 5. Performance comparisons of the disturbance rejection (For the case of step responses).

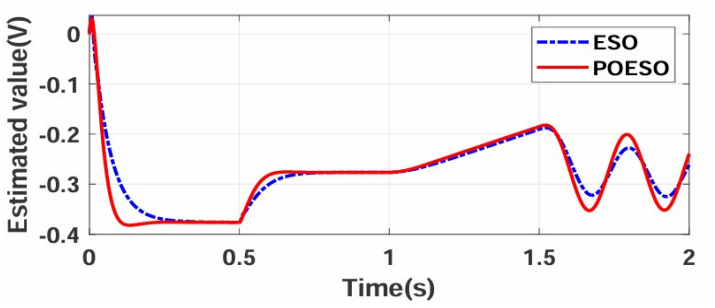

Figure 6. The generalized disturbance estimations (For the case of step responses).

4.2. Sinusoidal Responses (I)

A 5 Hz sinusoidal trajectory is taken as the set-value. Results are shown in Figure 7. RMS values of tracking errors and control signals are listed in Table 3. The POADRC consumes minimal energy to get the best tracking accuracy. Hysteresis loops suppressed by the PI, ADRC, and POADRC are presented in Figure 8. The POADRC also behaves best. From Figure 7 and the data listed in Table 3, one can find that the POADRC tracks the time-varying reference best. Similar to Figure 6, Figure 9 presents a POESO's phase advantage on the generalized disturbance estimation. Next, another sinusoidal reference is selected to test the system's high-speed motion.

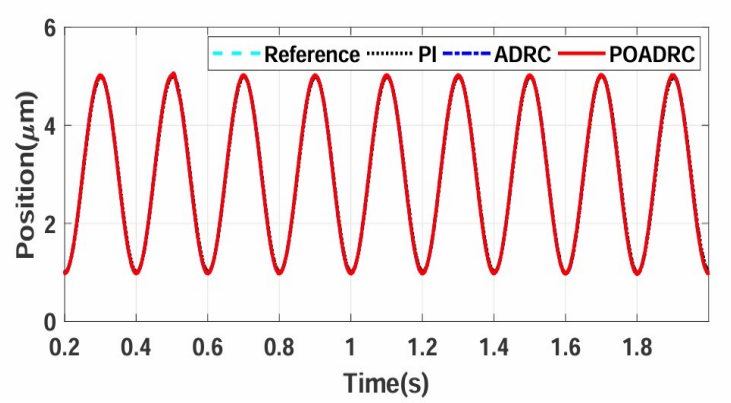

(**a**)

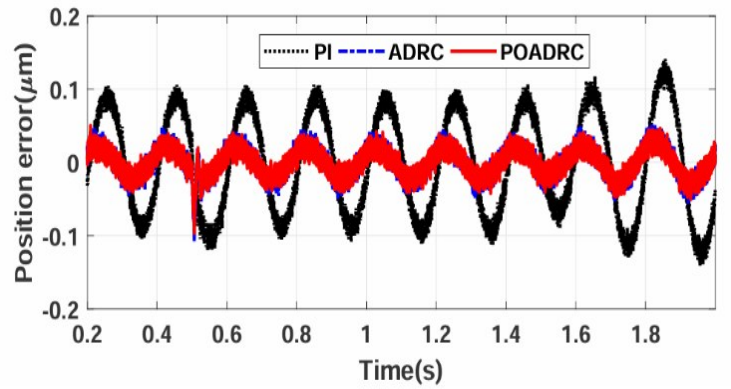

(**b**)

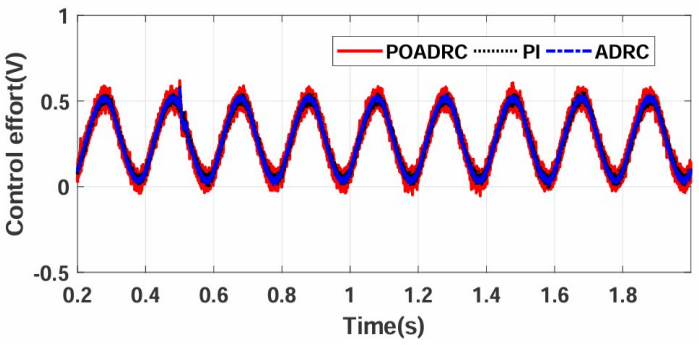

(**c**)

Figure 7. 5 Hz sinusoidal motion tracking results. (**a**) Position tracking results. (**b**) Position tracking errors. (**c**) Control efforts.

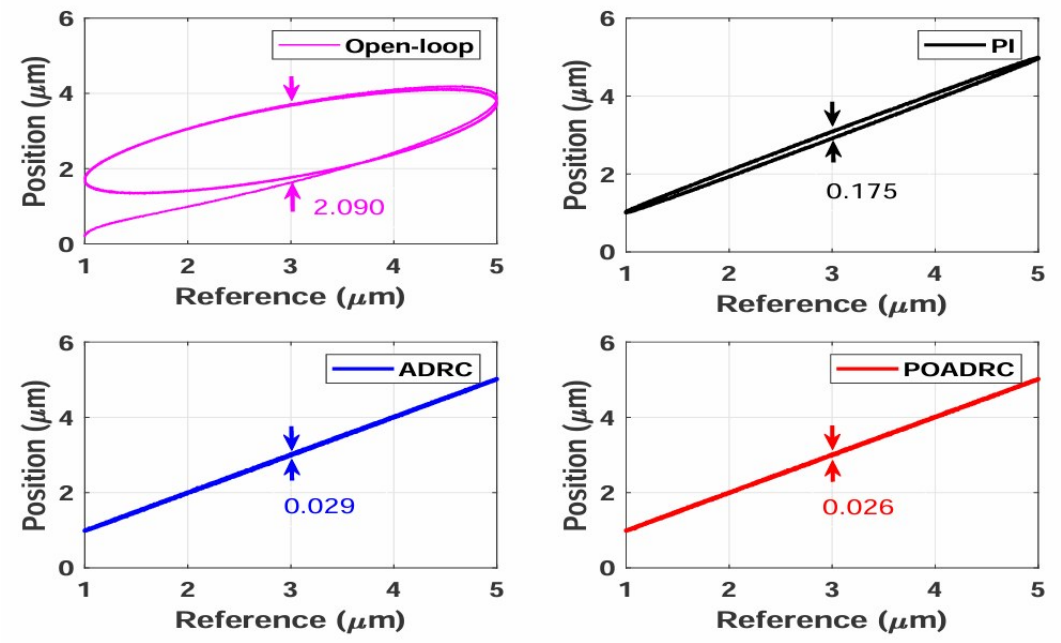

Figure 8. Hysteresis curves by different control approaches (For the case of 5 Hz sinusoidal reference).

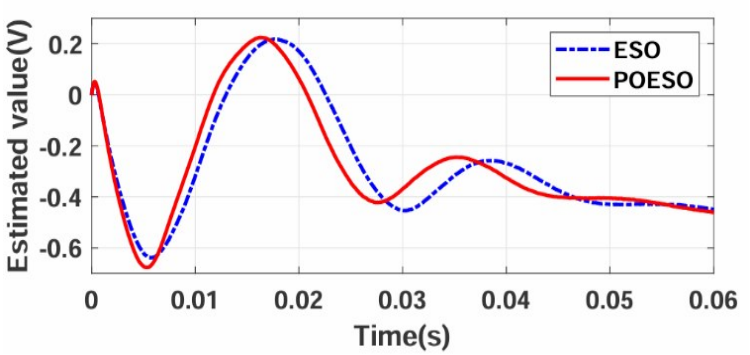

Figure 9. The generalized disturbance estimations (For the case of 5 Hz sinusoidal tracking responses).

4.3. Sinusoidal Responses (II)

Generally, a system runs at around 1/100 to 1/10 of the lowest resonant-vibrational frequency [34]. It does limit the operating speed and motivates a high-bandwidth positioning. Here, a 20 Hz sinusoidal reference, whose frequency exceeds 10% of the stage's resonant frequency (190 Hz), is taken. The sampling interval is 0.06 ms. The tracking results are shown in Figure 10. Figure 10a shows tracking performance of the three control strategies. From Figure 10b, one can see the POADRC has the minimum tracking errors. Figure 10c presents facts that the POADRC's control signals lead the ones of the ADRC and the PI, and the ADRC's control signals are ahead of the ones of the PI. In other words, the POADRC is the most active regulation, and the PI is the most passive one. Accordingly, positioning errors shown in Figure 10b agrees with the control signals presented in Figure 10c. In addition, Figure 11 shows hysteresis curves compensated by the PI, the ADRC, and the POADRC. Apparently, the estimation phase advantage of the POESO shown in Figure 12 guarantees the POADRC provides the most active control and behaves best.

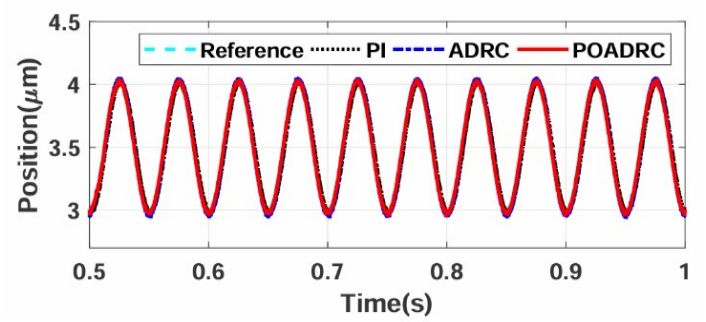

(**a**)

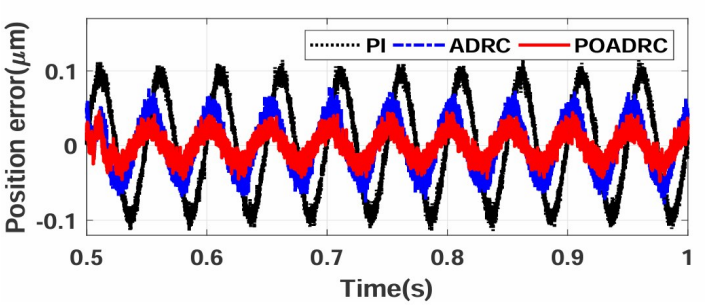

(**b**)

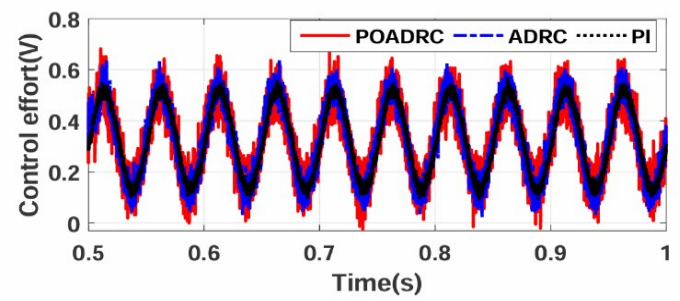

(**c**)

Figure 10. 20 Hz sinusoidal motion tracking results. (**a**) Position tracking results. (**b**) Position tracking errors. (**c**) Control efforts.

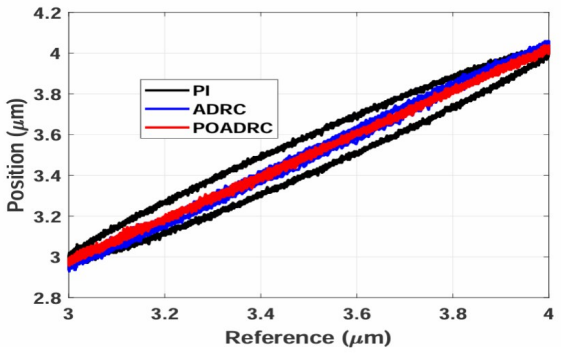

Figure 11. Hysteresis curves by different control approaches (For the case of 20 Hz sinusoidal reference).

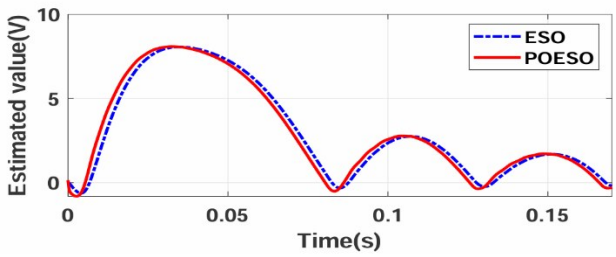

Figure 12. The generalized disturbance estimations (For the case of 20 Hz sinusoidal tracking responses).

5. Conclusions

The POESO and the POADRC are designed, analyzed, and verified in this article. Instead of introducing linearities, nonlinearities or raising order, a POESO is realized by a straightforward and effective modification to a classical ESO. Experimental results show that the POESO ensures better positioning performance. It is practical and efficient. Nevertheless, parameter 'c' still needs a standard/systematic optimization. Furthermore, providing a leading generalized disturbance estimation phase may be a promising way to improve the ESO based ADRC approaches. It deserves further investigations.

Author Contributions: Conceptualization, W.W.; methodology, W.W., and P.X.; software, P.X.; validation, P.X., W.W., and M.Z.; formal analysis, W.W., P.X., and M.Z.; investigation, P.X.; resources, W.W., and M.Z.; data curation, P.X.; writing—original draft preparation, P.X., and W.W.; writing—review and editing, W.W., and P.X.; visualization, P.X., and W.W.; supervision, W.W.; project administration, W.W., and M.Z.; funding acquisition, W.W. All authors have read and agreed to the published version of the manuscript.

Funding: This work was supported by the National Natural Science Foundation of China (61403006, 61873005), and the Open Project Program of National Engineering Laboratory for Agri-product Quality Traceability, grant number AQT-2021-YB2.

Institutional Review Board Statement: Not applicable.

Informed Consent Statement: Not applicable.

Data Availability Statement: Not applicable.

Conflicts of Interest: The authors declare no conflict of interest.

Appendix A

Appendix A.1. Proof of Theorem 1

Proof of Theorem 1. Solving (10), one has

$$\varepsilon_{PO}(t) = e^{\omega_o \mathbf{A}_\varepsilon t}\varepsilon_{PO}(0) + \int_0^t e^{\omega_o \mathbf{A}_\varepsilon (t-\tau)}\mathbf{B}_\varepsilon \frac{h(\tau)}{\omega_o^2} d\tau \tag{28}$$

Let

$$p(t) = \int_0^t e^{\omega_o \mathbf{A}_\varepsilon (t-\tau)}\mathbf{B}_\varepsilon \frac{h(\tau)}{\omega_o^2} d\tau = \left[p_1, p_2, p_3\right]^T \tag{29}$$

Since $h(t)$ is bounded, i.e., $h(t) \le \delta$, here δ is a positive constant, it follows that

$$\left| p_i(t) \right| \le \frac{\delta}{\omega_o^3}\left(\left| \left(\mathbf{A}_\varepsilon^{-1}\mathbf{B}_\varepsilon\right)_i \right| + \left| \left(\mathbf{A}_\varepsilon^{-1} e^{\omega_o \mathbf{A}_\varepsilon t}\mathbf{B}_\varepsilon\right)_i \right| \right) \tag{30}$$

for $i = 1, 2, 3$. Since $\mathbf{A}_\varepsilon^{-1} = \begin{bmatrix} -3 & 0 & -1 \\ -8 & 0 & -3 \\ 0 & 1 & 0 \end{bmatrix}$, one has

$$\left| \left(\mathbf{A}_\varepsilon^{-1}\mathbf{B}_\varepsilon\right)_i \right| = \begin{cases} 1, & i = 1 \\ 3, & i = 2 \\ 0, & i = 3 \end{cases} \tag{31}$$

Since $\mathbf{A}_\varepsilon$ is Hurwitz, there exists a finite time $T_1 > 0$ such that

$$\left| \left[e^{\omega_o \mathbf{A}_\varepsilon t} \right]_{ij} \right| \le \frac{1}{\omega_o^3} \tag{32}$$

for $\forall t > T_1, i,j = 1,2,3$. Then,

$$\left| \left[e^{\omega_o \mathbf{A}_\varepsilon t} \mathbf{B} \right]_i \right| \le \frac{1}{\omega_o^3} \tag{33}$$

for $\forall t > T_1, i = 1,2,3$. Here, T_1 depends on $\omega_o \mathbf{A}_\varepsilon$.

Let $\mathbf{A}_\varepsilon^{-1} = \begin{bmatrix} a_{11} & a_{12} & a_{13} \\ a_{21} & a_{22} & a_{23} \\ a_{31} & a_{32} & a_{33} \end{bmatrix}$, $e^{\omega_o \mathbf{A}_\varepsilon t} = \begin{bmatrix} b_{11} & b_{12} & b_{13} \\ b_{21} & b_{22} & b_{23} \\ b_{31} & b_{32} & b_{33} \end{bmatrix}$, one has

$$\left| \left(\mathbf{A}_\varepsilon^{-1} e^{\omega_o \mathbf{A}_\varepsilon t} \mathbf{B}_\varepsilon \right)_i \right| \le \left| \sum_{j=1}^{3} a_{ij} b_{j3} \right| \le \begin{cases} \dfrac{4}{\omega_o^3}, & i = 1 \\ \dfrac{11}{\omega_o^3}, & i = 2 \\ \dfrac{1}{\omega_o^3}, & i = 3 \end{cases} \tag{34}$$

for $\forall t > T_1$. From (30), (31), and (34), one has

$$\left| p_i(t) \right| \le \begin{cases} \dfrac{\delta}{\omega_o^3} + \dfrac{4\delta}{\omega_o^6}, & i = 1 \\ \dfrac{3\delta}{\omega_o^3} + \dfrac{11\delta}{\omega_o^6}, & i = 2 \\ \dfrac{\delta}{\omega_o^6}, & i = 3 \end{cases} \tag{35}$$

for $\forall t > T_1, i = 1,2,3$.

Let $\varepsilon_m(0) = \left| \varepsilon_1(0) \right| + \left| \varepsilon_2(0) \right| + \left| \varepsilon_{3PO}(0) \right|$, then

$$\left| \left[e^{\omega_o \mathbf{A}_\varepsilon t} \varepsilon_{PO}(0) \right]_i \right| \le \frac{\varepsilon_m(0)}{\omega_o^3} \tag{36}$$

for $\forall t > T_1, i = 1,2,3$. From (28), one has

$$\left| \varepsilon_{PO}(t) \right| \le \left| \left[e^{\omega_o \mathbf{A}_\varepsilon t} \varepsilon_{PO}(0) \right] \right| + \left| \boldsymbol{p}(t) \right| \tag{37}$$

According to (35)–(37), one has

$$\left| \left[\varepsilon_{PO}(t) \right]_i \right| = \begin{cases} \dfrac{\varepsilon_m(0)}{\omega_o^3} + \dfrac{\delta}{\omega_o^3} + \dfrac{4\delta}{\omega_o^6}, & i = 1 \\ \dfrac{\varepsilon_m(0)}{\omega_o^3} + \dfrac{3\delta}{\omega_o^3} + \dfrac{11\delta}{\omega_o^6}, & i = 2 \\ \dfrac{\varepsilon_m(0)}{\omega_o^3} + \dfrac{\delta}{\omega_o^6}, & i = 3 \end{cases} \tag{38}$$

for $\forall t > T_1, i = 1,2,3$.

Let $e_m(0) = \left| e_1(0) \right| + \left| e_2(0) \right| + \left| e_{3PO}(0) \right|$, then

$$\begin{cases} e_1(t) \le \dfrac{e_m(0)}{\omega_o^3} + \dfrac{\delta}{\omega_o^3} + \dfrac{4\delta}{\omega_o^6} = \sigma_1 \\ e_2(t) \le \dfrac{e_m(0)}{\omega_o^2} + \dfrac{3\delta}{\omega_o^2} + \dfrac{11\delta}{\omega_o^5} = \sigma_2 \\ e_{3PO}(t) \le \dfrac{e_m(0)}{\omega_o} + \dfrac{\delta}{\omega_o^4} = \sigma_3 \end{cases} \tag{39}$$

for $\forall t > T_1$.□

Appendix A.2. Proof of Theorem 2

Proof of Theorem 2. From (6) and definitions of the tracking errors and the estimation errors, one has

$$u = \frac{k_p(\xi_1 - e_1) + k_d(\xi_2 - e_2) + (r_3 - x_3 - e_{3PO})}{b_0} \tag{40}$$

and

$$\begin{cases} \dot{\xi}_1 = \dot{r}_1 - \dot{x}_1 = r_2 - x_2 = \xi_2 \\ \dot{\xi}_2 = -k_p\xi_1 - k_d\xi_2 + \left(k_p - \dfrac{\beta_3}{c}\right)e_1 + k_d e_2 + e_3 \end{cases} \tag{41}$$

From (8), one has $\beta_3 = \omega_o^3$. Let $\boldsymbol{\xi}(t) = \left[\xi_1(t), \xi_2(t)\right]^T$, $e(t) = \left[e_1(t), e_2(t), e_3(t)\right]^T$, and $c = \omega_o/3$, one has

$$\dot{\boldsymbol{\xi}}(t) = \mathbf{A}_\xi \boldsymbol{\xi}(t) + \mathbf{A}_\mathrm{e} e(t) \tag{42}$$

where $\mathbf{A}_\xi = \begin{bmatrix} 0 & 1 \\ -k_p & -k_d \end{bmatrix}$, $\mathbf{A}_\mathrm{e} = \begin{bmatrix} 0 & 0 & 0 \\ k_p - 3\omega_o^2 & k_d & 1 \end{bmatrix}$.

Solving (42), it follows that

$$\boldsymbol{\xi}(t) = e^{\mathbf{A}_\xi t}\boldsymbol{\xi}(0) + \int_0^t e^{\mathbf{A}_\xi(t-\tau)}\mathbf{A}_\mathrm{e} e(\tau)\,d\tau \tag{43}$$

For $\boldsymbol{A}_\mathrm{e}\boldsymbol{e}(\tau) = \left[0, \quad \left(k_p - 3\omega_o^2\right)e_1(\tau) + k_d e_2(\tau) + e_3(\tau)\right]^T$, according to Theorem 1, $\forall t \ge T_1$, one has

$$\left(\mathbf{A}_\mathrm{e} e\right)_2 \le k_p\sigma_1 + k_d\sigma_2 + \sigma_3 \triangleq \gamma \tag{44}$$

Let $\varphi(t) = \int_0^t e^{\mathbf{A}_\xi(t-\tau)}\mathbf{A}_\mathrm{e} e(\tau)\,d\tau$, $\boldsymbol{\theta} = \left[0, \gamma\right]^T$, it follows that

$$\left|\varphi_i(t)\right| \le \left|\left(\mathbf{A}_\xi^{-1}\boldsymbol{\theta}\right)_i\right| + \left|\left(\mathbf{A}_\xi^{-1}e^{\mathbf{A}_\xi t}\boldsymbol{\theta}\right)_i\right| \tag{45}$$

Taking (7) into consideration, one has

$$\left|\left(\mathbf{A}_\xi^{-1}\boldsymbol{\theta}\right)_i\right| = \begin{cases} \dfrac{\gamma}{\omega_c^2}, & i = 1 \\ 0, & i = 2 \end{cases} \tag{46}$$

when $\mathbf{A}_\xi$ is Hurwitz, there exists a finite time $T_2 > 0$ such that

$$\left|\left[e^{\mathbf{A}_\xi t}\right]_{ij}\right| \le \frac{1}{\omega_c^3} \tag{47}$$

for $\forall t \ge T_2$, $i, j = 1, 2$.

Note that T_2 depends on $\mathbf{A}_\xi$. Let $e^{\mathbf{A}_\xi t} = \begin{bmatrix} \rho_{11} & \rho_{12} \\ \rho_{21} & \rho_{22} \end{bmatrix}$ and $\xi_m(0) = \left|\xi_1(0)\right| + \left|\xi_2(0)\right|$, it follows that

$$\left|\left[e^{\mathbf{A}_\xi t}\boldsymbol{\xi}(0)\right]_i\right| \le \frac{\xi_m(0)}{\omega_c^3} \tag{48}$$

for $\forall t \geq T_2, i = 1, 2$.

$$\left| \left(e^{\mathbf{A}_\xi t} \boldsymbol{\theta} \right)_i \right| \leq \frac{\gamma}{\omega_c^3} \tag{49}$$

for $\forall t \geq T_3, i = 1, 2$, and Let $T_3 = \max\{T_1, T_2\}$, one has

$$\left| \left(\mathbf{A}_\xi^{-1} e^{\mathbf{A}_\xi t} \boldsymbol{\theta} \right)_i \right| \leq \begin{cases} \dfrac{\left(1 + 2\omega_c\right)}{\omega_c^2} \cdot \dfrac{\gamma}{\omega_c^3}, & i = 1 \\ \dfrac{\gamma}{\omega_c^3}, & i = 2 \end{cases} \tag{50}$$

for $\forall t \geq T_3$.

From (45), (46), and (50), one has

$$\left| \varphi_i(t) \right| \leq \begin{cases} \dfrac{\gamma}{\omega_c^2} + \dfrac{\left(1 + 2\omega_c\right)}{\omega_c^2} \cdot \dfrac{\gamma}{\omega_c^3}, & i = 1 \\ \dfrac{\gamma}{\omega_c^3}, & i = 2 \end{cases} \tag{51}$$

for $\forall t \geq T_3$. From (43), one has

$$\left| \xi_i(t) \right| \leq \left| \left[e^{\mathbf{A}_\xi t} \boldsymbol{\xi}(0) \right]_i \right| + \left| \varphi_i(t) \right| \tag{52}$$

According to (48), (51), and (52), one has

$$\left| \xi_i(t) \right| \leq \begin{cases} \dfrac{\xi_m(0)}{\omega_c^3} + \dfrac{\omega_c^2 \sigma_1 + 2\omega_c \sigma_2 + \sigma_3}{\omega_c^2} + \\ \dfrac{\left(1 + 2\omega_c\right)}{\omega_c^2} \cdot \dfrac{\omega_c^2 \sigma_1 + 2\omega_c \sigma_2 + \sigma_3}{\omega_c^3} & i = 1 \\ \dfrac{\xi_m(0) + \omega_c^2 \sigma_1 + 2\omega_c \sigma_2 + \sigma_3}{\omega_c^3} & i = 2 \end{cases} \tag{53}$$

for $\forall t \geq T_3, i = 1, 2$.

Let

$$\mu_i = \max \left\{ \begin{array}{l} \dfrac{\xi_m(0)}{\omega_c^3} + \dfrac{\omega_c^2 \sigma_1 + 2\omega_c \sigma_2 + \sigma_3}{\omega_c^2} + \\ \dfrac{\left(1 + 2\omega_c\right)}{\omega_c^2} \cdot \dfrac{\omega_c^2 \sigma_1 + 2\omega_c \sigma_2 + \sigma_3}{\omega_c^3}, \\ \dfrac{\xi_m(0) + \omega_c^2 \sigma_1 + 2\omega_c \sigma_2 + \sigma_3}{\omega_c^3} \end{array} \right\} \tag{54}$$

then $\left| \xi_i(t) \right| \leq \mu_i, i = 1, 2, \forall t \geq T_3 > 0, \omega_o > 0, \omega_c > 0$. □

References

1. Devasia, S.; Eleftheriou, E.; Moheimani, S.O.R. A survey of control issues in nanopositioning. *IEEE Trans. Control Syst. Technol.* **2007**, *15*, 802–823.
2. Gu, G.; Zhu, L.; Su, C.; Ding, H.; Fatikow, S. Modeling and control of piezo-actuated nanopositioning stages: A survey. *IEEE Trans. Autom. Sci. Eng.* **2016**, *13*, 313–332.
3. Mishra, J. P.; Xu, Q.; Yu, X.; Jalili, M. Precision position tracking for piezoelectric-driven motion system using continuous third-order sliding mode control. *IEEE/ASME Trans. Mechatron.* **2018**, *23*, 1521–1531.
4. Shan, L.; Yang, X.; Yao, L.; Ning, L. Research on modelling of piezoelectric micro-positioning stage based on pi hysteresis model. *J. Eng.* **2019**, *2019*, 437–441.
5. Gu, G.; Li, C.; Zhu, L.; Su, C. Modeling and identification of piezoelectric-actuated stages cascading hysteresis nonlinearity with linear dynamics. *IEEE/ASME Trans. Mechatron.* **2016**, *21*, 1792–1797.

6. Li, Z.; Shan, J.; Gabbert, U. Dynamics modeling and inversion-based synchronized model predictive control for a fabry-perot spectrometer. *IEEE/ASME Trans. on Mechatron.* **2019**, *24*, 1818–1828.
7. Liu, X.; Huang, M.; Xiong, R.; Shan, J.; Mao, X. Adaptive inverse control of piezoelectric actuators based on segment similarity. *IEEE Trans. Ind. Electron.* **2018**, *66*, 5403–5411.
8. Jian, Y.; Huang, D.; Liu, J.; Min, D. High-precision tracking of piezoelectric actuator using iterative learning control and direct inverse compensation of hysteresis. *IEEE Trans. Ind. Electron.* **2018**, *66*, 368–377.
9. Rakotondrabe, M. Bouc-wen modeling and inverse multiplicative structure to compensate hysteresis nonlinearity in piezoelectric actuators. *IEEE Trans. Autom. Sci. Eng.* **2010**, *8*, 428–431.
10. Lin, C. J.; Lin, P. Tracking control of a biaxial piezo-actuated positioning stage using generalized duhem model. *Comput. Math. Appl.* **2012**, *64*, 766–787.
11. Piao, M.; Wang, Y.; Sun, M.; Zhang, X.; Chen, Z.; Yan, Y. Fixed-time-convergent generalized extended state observer based motor control subject to multiple disturbances. *IEEE Trans. Ind. Inf.* **2021**, *17*, 8066–8079.
12. Na, J.; Jing, B.; Huang, Y.; Gao, G.; Zhang C. Unknown system dynamics estimator for motion control of nonlinear robotic systems. *IEEE Trans. Ind. Electron.* **2020**, *67*, 3850–3859.
13. Sun, J.L.; He, H.B.; Yi, J.Q.; Pu, Z.Q. Finite-time command-filtered composite adaptive neural control of uncertain nonlinear systems. *IEEE Trans. Cybern.* **2020**, *52*, 6809–6821. https://doi.org/10.1109/TCYB.2020.3032096.
14. de Rozario, R.; Fleming, A.; Oomen, T. Finite-time learning control using frequency response data with application to a nanopositioning stage. *IEEE/ASME Trans. Mech.* **2019**, *5*, 2085–2096.
15. Liu, J.B.; Wang, J.R.; Zou, Q.Z. Decomposition-learning-based output tracking to simultaneous hysteresis and dynamics control: High-speed large-range nanopositioning example. *IEEE Trans. Control Syst. Technol.* **2021**, *29*, 1775 – 1782.
16. Kong, L. H.; Li, D.; Zou, J. X.; He, W. Neural networks based learning control for a piezoelectric nanopositioning system. *IEEE/ASME Trans. Mech.* **2020**, *25*, 2904–2914.
17. Han, J. From pid to active disturbance rejection control. *IEEE Trans. Ind. Electron.* **2009**, *56*, 900–906.
18. Zhang, Y. L.; Zhu, M.; Li, D. H.; Wang, J. Adrc dynamic stabilization of an unstable heat equation. *IEEE Trans. Autom. Control* **2020**, *65*, 4424–4429.
19. Gao, H.; Chen, Z.; Sun, M.; Huang, J.; Wang, Z.; Chen, Z. An efficient fast altitude control for hypersonic vehicle. *Control Eng. Pract.* **2020**, *100*, 10442601–10442613.
20. Tao, J.; Sun, Q.; Tan, P.; Chen, Z.; He, Y. Active disturbance rejection control (adrc)-based autonomous homing control of powered parafoils. *Nonlinear Dyn.* **2016**, *86*, 1461–1476.
21. Jiang, Y.; Sun, Q.; Zhang, X.; Chen, Z. Pressure regulation for oxygen mask based on active disturbance rejection control. *IEEE Trans. Ind. Electron.* **2017**, *64*, 6402–6411.
22. Cheng, Y.; Chen, Z.; Sun, M.; Sun, Q. Cascade active disturbance rejection control of a high-purity distillation column with measurement noise. *Ind. Eng. Chem. Res.* **2018**, *57*, 4623–4631.
23. Zarif Mansour, S.; Seethaler, R. J.; Teo, Y. R.; Yong, Y. K.; Fleming, A. J. Piezoelectric bimorph actuator with integrated strain sensing electrodes. *IEEE Sens. J.* **2018**, *18*, 5812–5817.
24. Wang, G.; Xu, Q. Sliding mode control with disturbance rejection for piezoelectric nanopositioning control. In Proceedings of the 2018 Annual American Control Conference (ACC), Milwaukee, WI, USA, 27–29 June 2018; pp. 6144–6149.
25. Tan, K.K.; Lee, T.H.; Zhou, H.X. Micro-positioning of linear- piezoelectric motors based on a learning nonlinear pid controller. *IEEE/ASME Trans. Mechatron.* **2001**, *6*, 428–436.
26. Madonski, R.; Herman, P. Survey on methods of increasing the efficiency of extended state disturbance observers. *ISA Trans.* **2015**, *56*, 18–27.
27. Madonski, R.; Łakomy, K.; Stankovic, M.; Shao, S.; Yang, J.; Li, S. Robust converter-fed motor control based on active rejection of multiple disturbances. *Control Eng. Pract.* **2021**, 107, 104696.
28. Stanković, M.R.; Madonski, R.; Shao, S.; Mikluc, D. On dealing with harmonic uncertainties in the class of active disturbance rejection controllers. *Int. J. Control* **2021**, *94*, 2795–2810.
29. Pu, Z.; Yuan, R.; Yi, J.; Tan, X. A class of adaptive extended state observers for nonlinear disturbed systems. *IEEE Trans. Ind. Electron.* **2015**, *62*, 5858–5869.
30. Wei, W.; Zhang, Z.; Zuo, M. Phase leading active disturbance rejection control for a nanopositioning stage. *ISA Trans.* **2021**, *116*, 218–231.
31. Gao, Z. Scaling and bandwidth-parameterization based controller tuning. In Proceedings of the 2003 American Control Conference, Denver, CO, USA, 4–6 June 2003; Volume 6; pp. 4989–4996.
32. Zheng, Q.; Chen, Z.; Gao, Z. A practical approach to disturbance decoupling control. *Control Eng. Pract.* **2009**, *17*, 1016 – 1025.
33. Chen, S.; Xue, W.; Huang, Y. On active disturbance rejection control for nonlinear systems with multiple uncertainties and nonlinear measurement. *Int. J. Robust Nonlinear Control* **2020**, *30*, 3411–3435.
34. Clayton, G.; Tien, S.; Leang, K.; Zou, Q.; Devasia S. A review of feedforward control approaches in nanopositioning for high-speed SPM. *J. Dyn. Syst. Meas. Control* **2009**, *131*, 061101–061119.